Available online at www.sciencedirect.com
SCIENCE DIRECT®
International Journal of Heat and Mass Transfer 49 (2006) 2712–2723
International Journal of HEAT and MASS TRANSFER
www.elsevier.com/locate/ijhmt

A finite difference method for studying thermal deformation in a thin film exposed to ultrashort-pulsed lasers

Haojie Wang [a], Weizhong Dai [a,*], Raja Nassar [a], Roderick Melnik [b]

[a] *Mathematics and Statistics, College of Engineering and Science, Louisiana Tech University, Ruston, LA 71272, USA*
[b] *Mathematical Modelling and Computational Sciences, Wilfrid Laurier University, Waterloo, Ont., Canada N2L 3C5*

Received 8 September 2005; received in revised form 9 January 2006
Available online 9 March 2006

Abstract

Ultrashort-pulsed lasers have been attracting worldwide interest in science and engineering. Studying the thermal deformation induced by ultrashort-pulsed lasers is important for preventing thermal damage. This article presents a finite difference method for studying thermal deformation in a thin film exposed to ultrashort-pulsed lasers. The method is obtained based on the parabolic two-step model. It accounts for the coupling effect between lattice temperature and strain rate, as well as for the hot-electron-blast effect in momentum transfer. The method allows us to avoid non-physical oscillations in the solution as demonstrated by numerical examples.

1. Introduction

Ultrafast lasers with pulse durations of the order of subpicoseconds to femtoseconds possess exclusive capabilities in limiting the undesirable spread of the thermal process zone in the heated sample [1]. The application of ultrashort-pulsed lasers includes structural monitoring of thin metal films [2,3], laser micromachining and patterning [4], structural tailoring of microfilms [5], and laser synthesis and processing in thin film deposition [6]. Recent applications of ultrashort-pulsed lasers have been in different disciplines such as physics, chemistry, biology, medicine, and optical technology [7–10]. The non-contact nature of femtosecond lasers has made them an ideal candidate for precise thermal processing of functional nanophase materials [1].

Success of high-energy ultrashort-pulsed lasers in real applications relies on three factors [1]: (1) well characterized pulse width, intensity and experimental techniques; (2) reliable microscale heat transfer models; and (3) prevention of thermal damage. It should be pointed out here that ultrafast damage induced by sub-picosecond pulses is intrinsically different from that induced by long-pulse or continuous lasers. For the latter, laser damage is caused by elevated temperatures resulting from the continuous pumping of photon energy into the processed sample. Therefore, the "damage threshold" in heating by long-pulse lasers is often referred to as the laser intensity that drives the heated spot to the melting temperature. Thermal damage induced by ultrashort pulses in the picosecond domain, on the other hand, occurs after the heating pulse is over.

Up-to-date, there are many researchers studying heat transfer models related to ultrashort-pulsed lasers [11–22]. However, only a few mathematical models for studying thermal deformation induced by ultrashort-pulsed lasers have been developed [1,23–25]. Tzou and his colleagues [1] presented a one-dimensional model in a double-layered thin film. The model was solved using a differential-difference approach. Chen and his colleagues [23] considered a two-dimensional axisymmetric cylindrical thin film and proposed an explicit finite difference method by adding an artificial viscosity term to eliminate numerical oscillations. In this study, we consider a two-dimensional plain strain thin film model in rectangular coordinates. The film is

* Corresponding author. Tel.: +1 318 257 3301; fax: +1 318 257 2562.
E-mail address: dai@coes.latech.edu (W. Dai).

0017-9310/$ - see front matter © 2006 Elsevier Ltd. All rights reserved.
doi:10.1016/j.ijheatmasstransfer.2006.01.013

Nomenclature

C_{e0}	electron heat capacity
C_l	lattice heat capacity
G	electron–lattice coupling factor
J	laser fluence
K	bulk modulus
K_e	thermal conductivity
R	surface reflectivity
T_e	electron temperature
T_l	lattice temperature
t, t_n	time
t_p	laser pulse duration
u, v	displacements in x and y directions, respectively
u_{ij}^n	numerical solution of $u(x_i, y_j, t_n)$
v_1, v_2	velocity components in x and y directions, respectively
x, y	Cartesian coordinates
x_s	optical penetration depth
y_s	spatial profile parameter
α_T	thermal expansion coefficient
$\Delta t, \Delta x, \Delta y$	time increment and spatial step sizes, respectively
Δ_{-t}, δ_x	finite difference operators
$\varepsilon_x, \varepsilon_y$	normal strains in x and y directions, respectively
Λ	electron-blast coefficient
γ_{xy}	shear strain
λ	Lame's coefficient
μ	Lame's coefficient
ρ	density
σ_x, σ_y	normal stresses in x and y directions, respectively
σ_{xy}	shear stress

exposed to ultrashort-pulsed lasers. An implicit finite difference scheme on a staggered grid for studying thermal deformation induced by ultrashort-pulsed lasers is developed based on the parabolic two-step heat transport equations. It accounts for the coupling effect between lattice temperature and strain rate, as well as for the hot-electron-blast effect in momentum transfer. The developed methodology allows us to avoid non-physical oscillations in the solution as demonstrated by a series of numerical experiments.

2. Mathematical model

Consider a two-dimensional thin film in rectangular coordinates, which is exposed to ultrashort-pulsed lasers as shown in Fig. 1. The governing equations for studying thermal deformation in the thin film can be expressed as follows:

(1) *Dynamic equations of motion* [1,23,26]

$$\rho\frac{\partial^2 u}{\partial t^2} = \frac{\partial \sigma_x}{\partial x} + \frac{\partial \sigma_{xy}}{\partial y} + 2\Lambda T_e\frac{\partial T_e}{\partial x}, \tag{1}$$

$$\rho\frac{\partial^2 v}{\partial t^2} = \frac{\partial \sigma_{xy}}{\partial x} + \frac{\partial \sigma_y}{\partial y} + 2\Lambda T_e\frac{\partial T_e}{\partial y}, \tag{2}$$

where

$$\sigma_x = \lambda(\varepsilon_x + \varepsilon_y) + 2\mu\varepsilon_x - (3\lambda + 2\mu)\alpha_T(T_l - T_0), \tag{3}$$

$$\sigma_y = \lambda(\varepsilon_x + \varepsilon_y) + 2\mu\varepsilon_y - (3\lambda + 2\mu)\alpha_T(T_l - T_0), \tag{4}$$

$$\sigma_{xy} = \mu\gamma_{xy}, \tag{5}$$

$$\varepsilon_x = \frac{\partial u}{\partial x}, \quad \varepsilon_y = \frac{\partial v}{\partial y}, \quad \gamma_{xy} = \frac{\partial u}{\partial y} + \frac{\partial v}{\partial x}. \tag{6}$$

Here, u is the displacement in the thickness direction (x-direction) and v is the displacement in length direction (y-direction); ε_x and ε_y are the normal strains in the x and y directions, respectively; γ_{xy} is the shear strain; σ_x and σ_y are the normal stresses in the x and y directions, respectively; σ_{xy} is the shear stress; T_e and T_l are electron and lattice temperatures, respectively; T_0 is an initial temperature; ρ is density; Λ is electron-blast coefficient; $\lambda = K - \frac{2}{3}\mu$ [27] and μ are Lame's coefficients; and α_T is the thermal expansion coefficient.

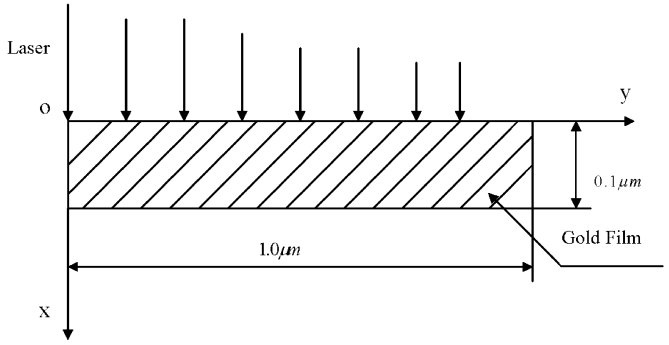

Fig. 1. Laser heating model.

(2) *Energy equations* [1,23,28]

$$C_e(T_e)\frac{\partial T_e}{\partial t} = \frac{\partial}{\partial x}\left[k_e(T_e, T_l)\frac{\partial T_e}{\partial x}\right] + \frac{\partial}{\partial y}\left[k_e(T_e, T_l)\frac{\partial T_e}{\partial y}\right] - G(T_e - T_l) + Q, \tag{7}$$

$$C_l\frac{\partial T_l}{\partial t} = G(T_e - T_l) - (3\lambda + 2\mu)\alpha_T\frac{\partial}{\partial t}(\varepsilon_x + \varepsilon_y), \tag{8}$$

where the heat source is given by

$$Q = 0.94J\frac{1-R}{t_p x_s}\exp\left[-\frac{x}{x_s} - \left(\frac{y}{y_s}\right)^2 - 2.77\left(\frac{t-2t_p}{t_p}\right)^2\right]. \tag{9}$$

Here, $C_e(T_e) = C_{e0}\left(\frac{T_e}{T_0}\right)$ is the electron heat capacity, $k_e(T_e, T_l) = k_0\left(\frac{T_e}{T_l}\right)$ is the thermal conductivity, G is the electron–lattice coupling factor, C_l is the lattice heat capacities, respectively; Q is energy absorption rate; J is laser fluence; R is surface reflectivity; t_p is laser pulse duration; x_s is

optical penetration depth; y_s is spatial profile parameter. Eqs. (7) and (8) are often referred to as parabolic two-step heat transport equations.

The boundary conditions are assumed to be

$$\sigma_x = 0, \quad \sigma_{xy} = 0, \quad \text{at } x = 0, L_x, \tag{10}$$

$$\sigma_y = 0, \quad \sigma_{xy} = 0, \quad \text{at } y = 0, L_y, \tag{11}$$

$$\frac{\partial T_e}{\partial \vec{n}} = 0, \quad \frac{\partial T_l}{\partial \vec{n}} = 0, \tag{12}$$

where $\vec{n}$ is the unit outward normal vector on the boundary. It should be pointed out that insulated boundaries are imposed due to the assumption that there are no heat losses from the film surfaces in the short time response.

The initial conditions are assumed to be

$$T_e = T_l = T_0, \quad u = v = 0, \quad u_t = v_t = 0, \quad \text{at } t = 0. \tag{13}$$

3. Finite difference method

In order to prevent the solution from oscillations, we introduce two velocity components v_1 and v_2 into the model and re-write the dynamic equations of motion, Eqs. (1)–(6), as follows:

$$v_1 = \frac{\partial u}{\partial t}, \quad v_2 = \frac{\partial v}{\partial t}, \tag{14}$$

$$\rho \frac{\partial v_1}{\partial t} = \frac{\partial \sigma_x}{\partial x} + \frac{\partial \sigma_{xy}}{\partial y} + \Lambda \frac{\partial T_e^2}{\partial x}, \tag{15}$$

$$\rho \frac{\partial v_2}{\partial t} = \frac{\partial \sigma_{xy}}{\partial x} + \frac{\partial \sigma_y}{\partial y} + \Lambda \frac{\partial T_e^2}{\partial y}, \tag{16}$$

$$\frac{\partial \varepsilon_x}{\partial t} = \frac{\partial v_1}{\partial x}, \quad \frac{\partial \varepsilon_y}{\partial t} = \frac{\partial v_2}{\partial y}, \quad \frac{\partial \gamma_{xy}}{\partial t} = \frac{\partial v_2}{\partial x} + \frac{\partial v_1}{\partial y}. \tag{17}$$

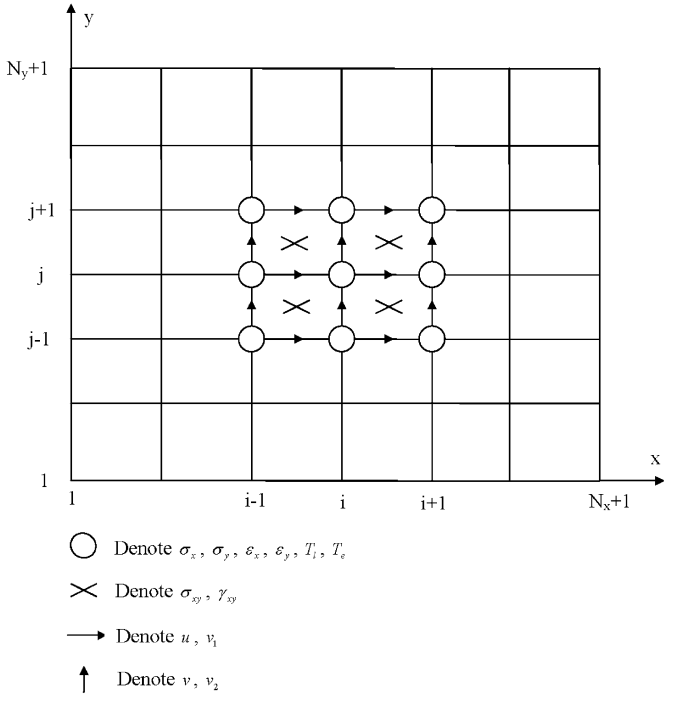

Fig. 2. A staggered mesh.

To develop a finite difference scheme, we first construct a staggered grid as shown in Fig. 2, where v_1 is placed at $(x_{i+1/2}, y_j)$, v_2 is placed at $(x_i, y_{j+1/2})$, γ_{xy} and σ_{xy} are placed at $(x_{i+1/2}, y_{j+1/2})$, while ε_x, ε_y, σ_x, σ_y, T_e and T_l are at (x_i, y_j). Here, i and j are indices with $1 \leqslant i \leqslant N_x + 1$ and $1 \leqslant j \leqslant N_y + 1$. We denote $v_1^n(i + 1/2, j)$ and $v_2^n(i, j + 1/2)$ as numerical approximations of $v_1((i + 1/2)\Delta x, j\Delta y, n\Delta t)$ and $v_2(i\Delta x, (j + 1/2)\Delta y, n\Delta t)$, respectively, where Δt, Δx and Δy are time increment and spatial step sizes, respectively. Similar notations are used for other variables. Furthermore, we introduce the finite difference operators, Δ_{-t}, δ_x and δ_x^2, as follows:

$$\Delta_{-t} u_j^n = u_j^n - u_j^{n-1}, \quad \delta_x u_j^n = u_{j+1/2}^n - u_{j-1/2}^n.$$

It should be pointed out that the staggered-grid method is often employed in computational fluid dynamics to prevent the solution from oscillations [29]. For example, if v_1 and ε_x in Eq. (17) are placed at a same location, employing a central finite difference scheme may produce a velocity component v_1, a wave solution, implying oscillation.

We now develop a finite difference method for solving the above governing equations. To this end, we first discretize equations (15) and (16) using a backward finite difference scheme as follows:

$$\begin{aligned} \rho \frac{1}{\Delta t} \Delta_{-t} v_1^{n+1}(i + 1/2, j) &= \frac{1}{\Delta x} \delta_x \sigma_x^{n+1}(i + 1/2, j) + \frac{1}{\Delta y} \delta_y \sigma_{xy}^{n+1}(i + 1/2, j) \\ &\quad + \Lambda \frac{1}{\Delta x} \delta_x (T_e^2)^{n+1}(i + 1/2, j), \end{aligned} \tag{18}$$

$$\begin{aligned} \rho \frac{1}{\Delta t} \Delta_{-t} v_2^{n+1}(i, j + 1/2) &= \frac{1}{\Delta x} \delta_x \sigma_{xy}^{n+1}(i, j + 1/2) + \frac{1}{\Delta y} \delta_y \sigma_y^{n+1}(i, j + 1/2) \\ &\quad + \Lambda \frac{1}{\Delta y} \delta_y (T_e^2)^{n+1}(i, j + 1/2), \end{aligned} \tag{19}$$

where Eq. (17) is discretized using backward finite differences as

$$\frac{1}{\Delta t} \Delta_{-t} \varepsilon_x^{n+1}(i, j) = \frac{1}{\Delta x} \delta_x v_1^{n+1}(i, j), \tag{20}$$

$$\frac{1}{\Delta t} \Delta_{-t} \varepsilon_y^{n+1}(i, j) = \frac{1}{\Delta y} \delta_y v_2^{n+1}(i, j), \tag{21}$$

$$\begin{aligned} \frac{1}{\Delta t} \Delta_{-t} \gamma_{xy}^{n+1}(i + 1/2, j + 1/2) &= \frac{1}{\Delta x} \delta_x v_2^{n+1}(i + 1/2, j + 1/2) + \frac{1}{\Delta y} \delta_y v_1^{n+1}(i + 1/2, j + 1/2), \end{aligned} \tag{22}$$

and Eqs. (3)–(5) are discretized as

$$\begin{aligned} \sigma_x^{n+1}(i, j) &= \lambda[\varepsilon_x^{n+1}(i, j) + \varepsilon_y^{n+1}(i, j)] + 2\mu \varepsilon_x^{n+1}(i, j) \\ &\quad - (3\lambda + 2\mu)\alpha_T [T_l^{n+1}(i, j) - T_0], \end{aligned} \tag{23}$$

$$\sigma_y^{n+1}(i,j) = \lambda[\varepsilon_x^{n+1}(i,j) + \varepsilon_y^{n+1}(i,j)] + 2\mu\varepsilon_y^{n+1}(i,j) - (3\lambda + 2\mu)\alpha_T[T_l^{n+1}(i,j) - T_0], \quad (24)$$

$$\sigma_{xy}^{n+1}(i+1/2, j+1/2) = \mu(\gamma_{xy}^{n+1}(i+1/2, j+1/2)). \quad (25)$$

We then discretize equations (7) and (8) using the Crank–Nicholson method as follows:

$$C_{e0}\left[\frac{T_e^{n+1}(i,j) + T_e^n(i,j)}{2}\right]\frac{1}{\Delta t}\Delta_{-t}T_e^{n+1}(i,j) = \frac{1}{2\Delta x^2}[k_e^{n+1}(i+1/2,j)\delta_x T_e^{n+1}(i+1/2,j) - k_e^{n+1}(i-1/2,j)\delta_x T_e^{n+1}(i-1/2,j)] + \frac{1}{2\Delta x^2}[k_e^n(i+1/2,j)\delta_x T_e^n(i+1/2,j) - k_e^n(i-1/2,j)\delta_x T_e^n(i-1/2,j)] + \frac{1}{2\Delta y^2}[k_e^{n+1}(i,j+1/2)\delta_x T_e^{n+1}(i,j+1/2) - k_e^{n+1}(i,j-1/2)\delta_x T_e^{n+1}(i,j-1/2)] + \frac{1}{2\Delta y^2}[k_e^n(i,j+1/2)\delta_x T_e^n(i,j+1/2) - k_e^n(i,j-1/2)\delta_x T_e^n(i,j-1/2)] - G\left[\frac{T_e^{n+1}(i,j) + T_e^n(i,j)}{2} - \frac{T_l^{n+1}(i,j) + T_l^n(i,j)}{2}\right] + Q^{n+\frac{1}{2}}(i,j), \quad (26)$$

Table 1
Thermophysical properties

Properties	Unit	Value
ρ	kg/m^3	19,300
Λ	J m^{-3} K^{-2}	70
K	Pa	217×10^9
μ	Pa	27×10^9
α_T	K^{-1}	14.2×10^{-6}
C_{e0}	J/(m^3 K)	2.1×10^4
C_l	J/(m^3 K)	2.5×10^6
G	W/(m^3 K)	2.6×10^6
K_e	W/(m K)	315
R		0.93
t_p	s	0.1×10^{-12}
x_s	m	15.3×10^{-9}
y_s	m	1.0×10^{-6}
J	J/m^2	500

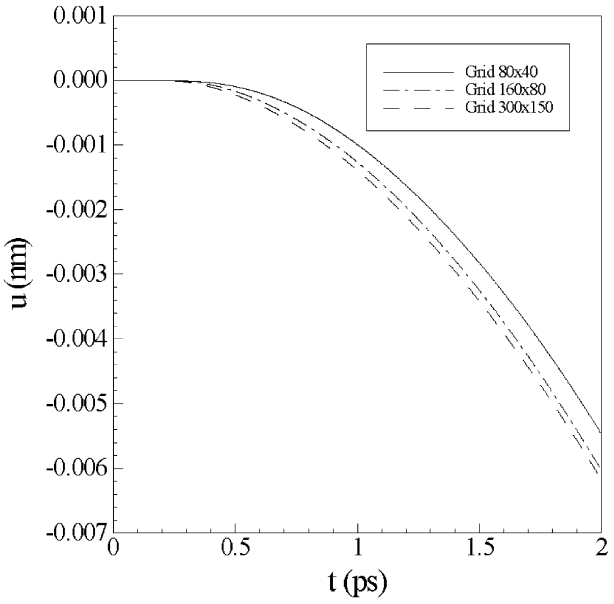

Fig. 4. Displacement (u) at $x = 0$ and $y = 0$ versus time for various meshes (80×40, 160×80, and 300×150).

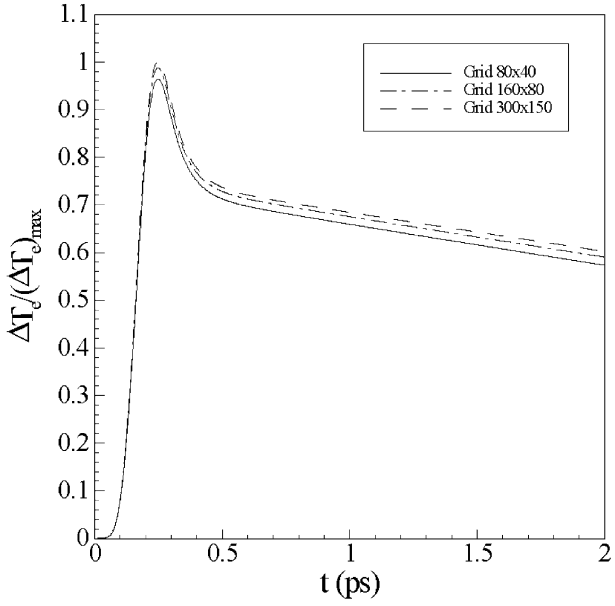

Fig. 3. Change in electron temperature at $x = 0$ and $y = 0$ versus time for various meshes (80×40, 160×80, and 300×150).

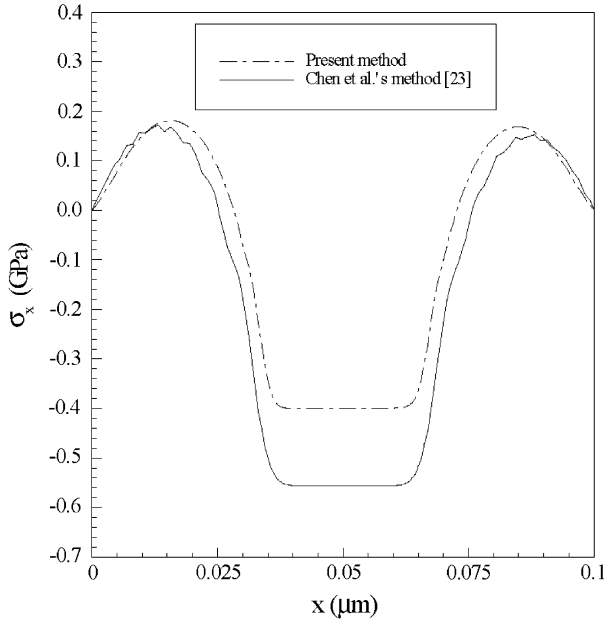

Fig. 5. Comparison of the present method with Chen et al.'s method in [23] with regard to the normal stress (σ_x) at $y = 0$ μm at $t = 10$ ps.

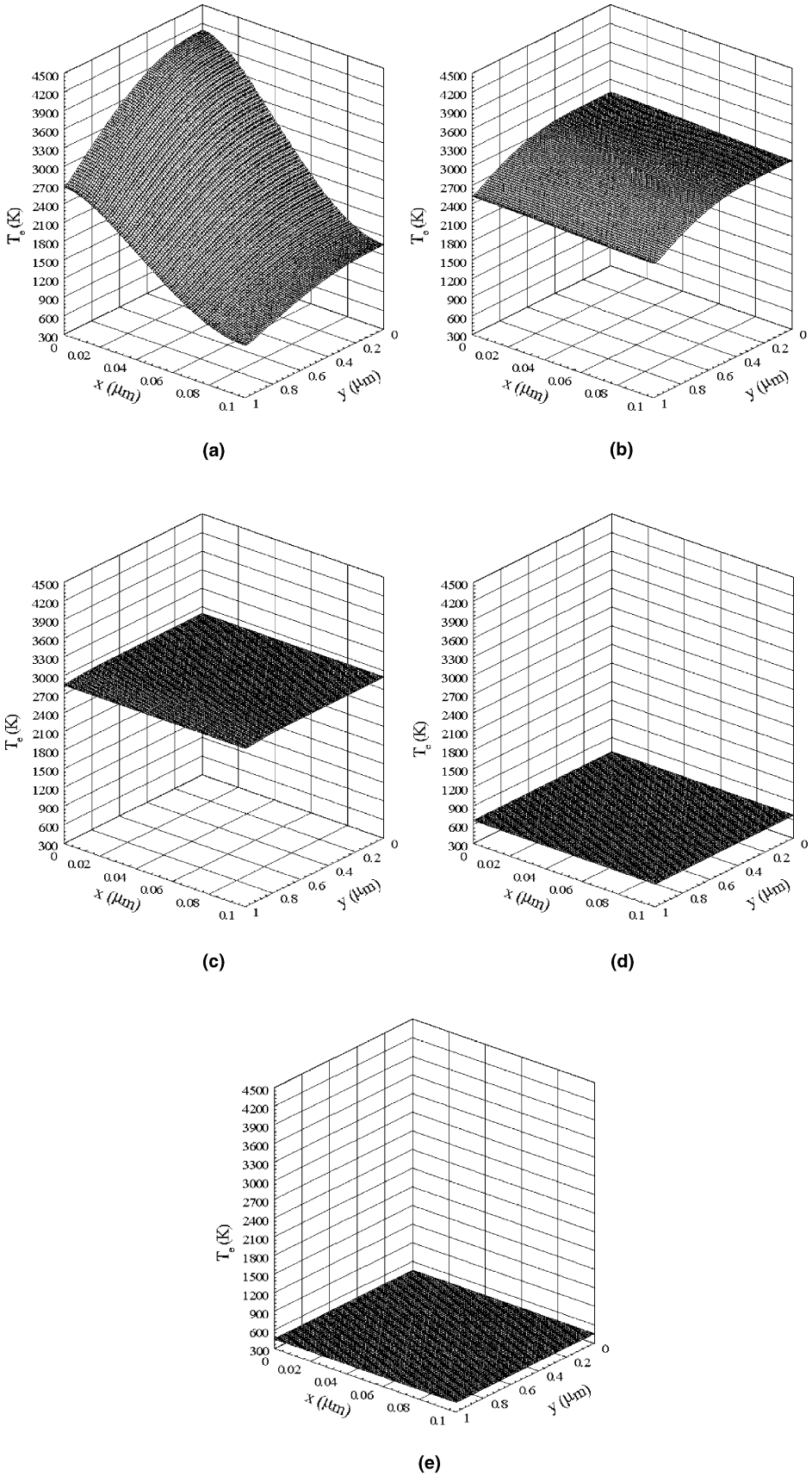

Fig. 6. Electron temperature profiles at (a) $t = 0.25$ ps, (b) $t = 0.5$ ps, (c) $t = 1$ ps, (d) $t = 10$ ps, and (e) $t = 20$ ps.

and

$$C_l\frac{1}{\Delta t}\Delta_{-t}T_l^{n+1}(i,j) = G\left[\frac{T_e^{n+1}(i,j)+T_e^n(i,j)}{2}-\frac{T_l^{n+1}(i,j)+T_l^n(i,j)}{2}\right] - (3\lambda+2\mu)\alpha_T\left[\frac{\Delta_{-t}\varepsilon_x^{n+1}(i,j)}{\Delta t}+\frac{\Delta_{-t}\varepsilon_x^n(i,j)}{\Delta t}\right]. \quad (27)$$

Finally, the displacements, u and v, are obtained using the Euler backward scheme for Eq. (14) as follows:

$$\Delta_{-t}u^{n+1}(i+1/2,j) = v_1^{n+1}(i+1/2,j), \quad (28)$$

$$\Delta_{-t}v^{n+1}(i,j+1/2) = v_2^{n+1}(i,j+1/2). \quad (29)$$

The boundary conditions, Eqs. (10)–(12), are discretized as follows:

$$\sigma_x^n(1,j)=0,\quad \sigma_x^n(N_x+1,j)=0,\quad 1\leqslant j\leqslant N_y+1, \quad (30a)$$

$$\sigma_{xy}^n(1+1/2,j+1/2)=0,\quad \sigma_{xy}^n(N_x+1/2,j+1/2)=0,\quad 1\leqslant j\leqslant N_y, \quad (30b)$$

$$\sigma_y^n(i,1)=0,\quad \sigma_y^n(i,N_y+1)=0,\quad 1\leqslant i\leqslant N_x+1, \quad (31a)$$

$$\sigma_{xy}^n(i+1/2,1+1/2)=0,\quad \sigma_{xy}^n(i+1/2,N_y+1/2)=0,\quad 1\leqslant i\leqslant N_x, \quad (31b)$$

$$T_e^n(1,j)=T_e^n(2,j),\quad T_e^n(N_x+1,j)=T_e^n(N_x,j),\quad 1\leqslant j\leqslant N_y+1, \quad (32a)$$

$$T_e^n(i,1)=T_e^n(i,2),\quad T_e^n(i,N_y+1)=T_e^n(i,N_y),\quad 1\leqslant i\leqslant N_x+1, \quad (32b)$$

$$T_l^n(1,j)=T_l^n(2,j),\quad T_l^n(N_x+1,j)=T_l^n(N_x,j),\quad 1\leqslant j\leqslant N_y+1, \quad (33a)$$

$$T_l^n(i,1)=T_l^n(i,2),\quad T_l^n(i,N_y+1)=T_l^n(i,N_y),\quad 1\leqslant i\leqslant N_x+1, \quad (33b)$$

for any time level n. The initial conditions are approximated as

$$u^0(i+1/2,j)=0,\quad v^0(i,j+1/2)=0, \quad (34a)$$

$$v_1^0(i+1/2,j)=0,\quad v_2^0(i,j+1/2)=0,\quad 1\leqslant i\leqslant N_x,\quad 1\leqslant j\leqslant N_y, \quad (34b)$$

$$T_e^0(i,j)=T_l^0(i,j)=T_0,\quad 1\leqslant i\leqslant N_x+1,\quad 1\leqslant j\leqslant N_y+1, \quad (34c)$$

$$\varepsilon_x^0(i,j)=\varepsilon_y^0(i,j)=0, \quad (34d)$$

$$\sigma_x^0(i,j)=\sigma_y^0(i,j)=0,\quad 1\leqslant i\leqslant N_x+1,\quad 1\leqslant j\leqslant N_y+1, \quad (34e)$$

$$\sigma_{xy}^0(i+1/2,j+1/2)=\gamma_{xy}^0(i+1/2,j+1/2)=0,\quad 1\leqslant i\leqslant N_x,\quad 1\leqslant j\leqslant N_y. \quad (34f)$$

It can be seen that the truncation error of Eqs. (18) and (19) is $O(\Delta t+\Delta x^2+\Delta y^2)$ and the truncation error of Eqs. (26) and (27) is $O(\Delta t^2+\Delta x^2+\Delta y^2)$. It should be pointed out that Eqs. (18) and (19) are nonlinear since the terms $\delta_x(T_e^2)^{n+1}(i+1/2,j)$ and $\delta_y(T_e^2)^{n+1}(i,j+1/2)$ are nonlinear. Also, it can be seen that Eqs. (26) and (27) are nonlinear. Therefore, the above scheme must be solved iteratively. An iterative method for solving the above scheme at time level $n+1$ is developed as follows:

Step 1. Guess ε_x^{n+1}, ε_y^{n+1} and γ_{xy}^{n+1} by using the values of ε_x^n, ε_y^n and γ_{xy}^n, solve Eqs. (26) and (27) iteratively for T_e^{n+1} and T_l^{n+1}.
Step 2. Solve for σ_x^{n+1}, σ_y^{n+1}, σ_{xy}^{n+1} using Eqs. (23)–(25).
Step 3. Solve for v_1^{n+1} and v_2^{n+1} using Eqs. (18) and (19).
Step 4. Update ε_x^{n+1}, ε_y^{n+1} and γ_{xy}^{n+1} using Eqs. (20)–(22).

Repeat the above steps until a convergent solution is obtained.

Note that the present method does not introduce an artificial viscosity term into the dynamic equations of motion. Recall that Chen et al.'s method [23] introduces an artificial viscosity term,

$$\Pi=\omega_L\rho V_s\Delta\bar{x}(trD)-\rho(\omega_Q\Delta\bar{x})^2|trD|(trD), \quad (35)$$

into the dynamical equations of motion

$$\rho\frac{\partial^2 u}{\partial t^2}=\frac{\partial\sigma_x}{\partial x}+\frac{\partial\sigma_{xy}}{\partial y}+2\Lambda T_e\frac{\partial T_e}{\partial x}+\frac{\partial\Pi}{\partial x} \quad (36)$$

and

$$\rho\frac{\partial^2 v}{\partial t^2}=\frac{\partial\sigma_{xy}}{\partial x}+\frac{\partial\sigma_y}{\partial y}+2\Lambda T_e\frac{\partial T_e}{\partial y}+\frac{\partial\Pi}{\partial y}, \quad (37)$$

in order to suppress oscillations in the thermal stress wave. Here, $\Delta\bar{x}$ is a characteristic dimension, ω_L and ω_Q are constants, and the velocity gradients term trD is defined as

$$trD=\frac{\partial^2 u}{\partial x\partial t}+\frac{\partial^2 v}{\partial y\partial t}. \quad (38)$$

In the next section, we provide comparisons between the results obtained with Chen et al.'s procedure and the methodology proposed in this paper.

4. Numerical Example

To test the applicability of the developed numerical scheme, we investigated the temperature rise and deformation in a single-layered thin film with the dimensions 0.1 μm (thickness) × 1 μm (length), as shown in Fig. 1. The thermophysical properties for gold are listed in Table 1 [1,23,31]. Three meshes of 80×40, 160×80, 300×150 were chosen in order to test the convergence of the scheme. The time increment is 0.005 ps. The laser fluence was chosen to be $J=500$ J/m^2. The initial temperature T_0 is 300 K.

Fig. 3 shows the change in electron temperature $(\Delta T_e/(\Delta T_e)_{max})$ at $x=0$ and $y=0$. The maximum temperature rise of T_e (i.e., $(\Delta T_e)_{max}$) is about 3791 K, which is

very close to that obtained by Qiu and Tien [30]. Fig. 4 shows the displacement (u) at $x = 0$ and $y = 0$ versus time. It can be seen from both figures that the solutions are convergent as the mesh is getting finer.

Figs. 5–11 were plotted based on the results obtained in a mesh of 160×80 and $\Delta t = 0.005$ ps. Fig. 5 presents the results obtained with Chen et al.'s method [23] and the methodology developed in the present paper. In particular,

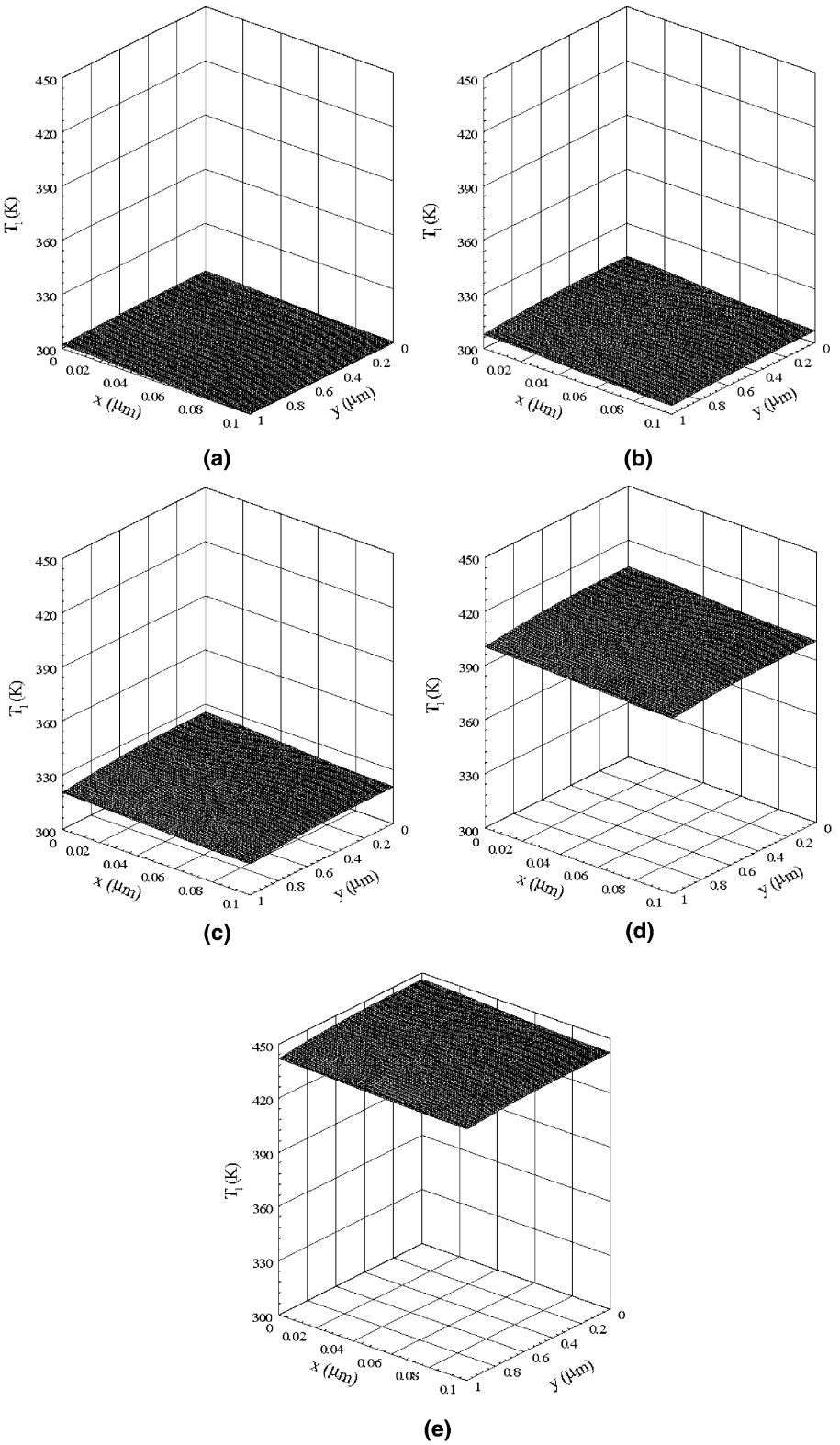

Fig. 7. Lattice temperature profiles at (a) $t = 0.25$ ps, (b) $t = 0.5$ ps, (c) $t = 1$ ps, (d) $t = 10$ ps, and (e) $t = 20$ ps.

we plotted the distribution of thermal stress σ_x at $y = 0$ μm when time $t = 10$ ps. The artificial viscosity approach by Chen et al. tends to overestimate the solution, as confirmed by Fig. 5. Furthermore, oscillations of the solution around two peaks, typical for this approach, are removed when the methodology developed here is applied. We also compared the computational cost between the present method and Chen et al.'s method. The present method took about 38 h of CPU time on a Dell computer (with Intel(R) Pentium(R) 4 CPU 1.60 GHz) to obtain the result at $t = 10$ ps while Chen et al.'s method took about 10 h. Obviously, the present method costs more computational time.

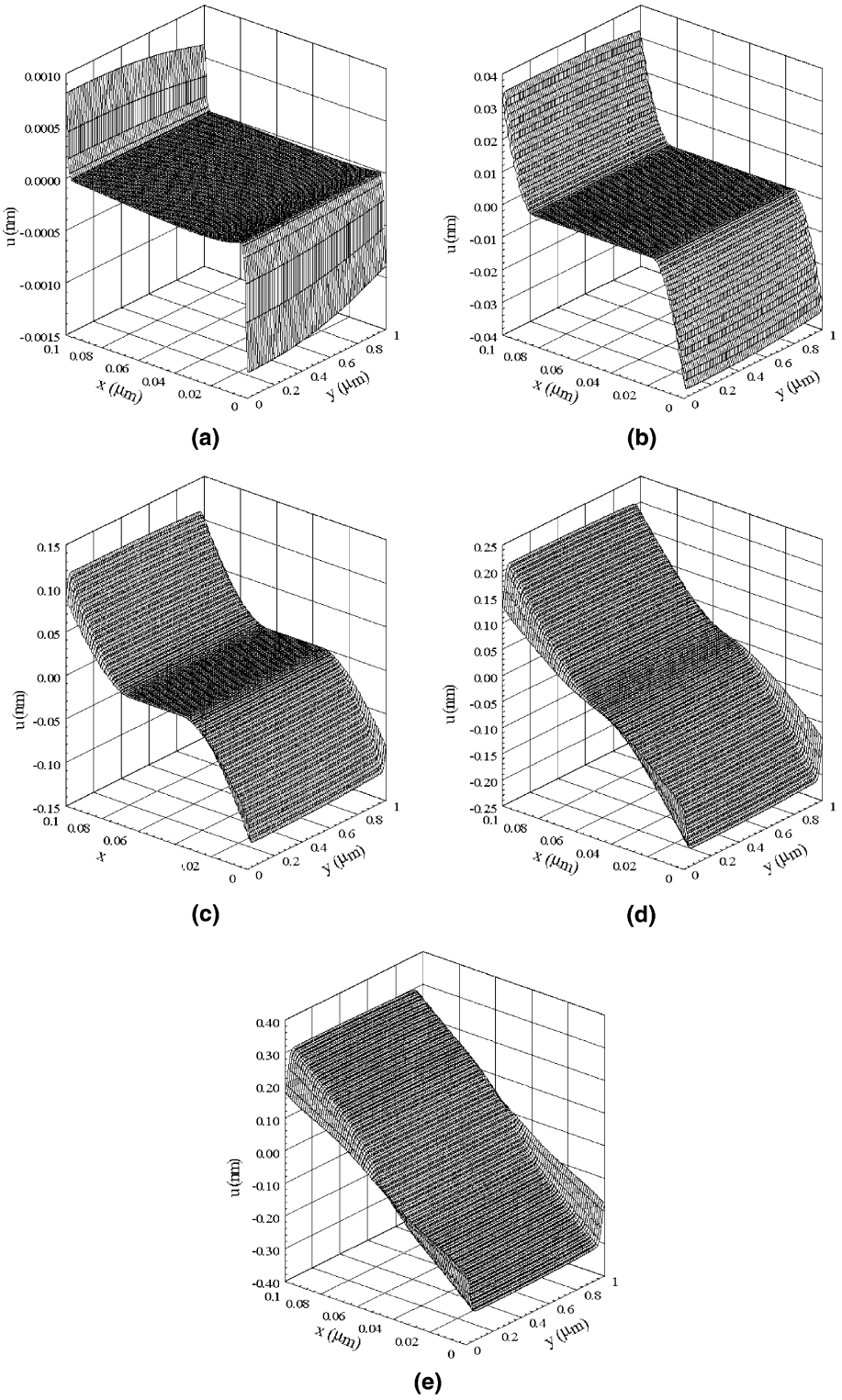

Fig. 8. Displacement (u) profiles at (a) $t = 1$ ps, (b) $t = 5$ ps, (c) $t = 10$ ps, (d) $t = 15$ ps, and (e) $t = 20$ ps.

This is because the present method is an implicit scheme and Chen et al.'s method is an explicit scheme.

Figs. 6 and 7 show respectively electron temperature and lattice temperature profiles at different times (a) $t = 0.25$ ps, (b) $t = 0.5$ ps, (c) $t = 1$ ps, (d) $t = 10$ ps, and (e) $t = 20$ ps. It can be seen that the electron temperature rises to its maximum at the beginning and then decreases to an uniform distribution at $t = 20$ ps while the lattice temperature rises gradually with time. Fig. 8 shows displacement u (thickness direction) profiles at different times (a) $t = 1$ ps, (b) $t = 5$ ps, (c) $t = 10$ ps, (d) $t = 15$ ps, and (e) $t = 20$ ps. Fig. 9 shows displacement v (length direction) profiles at different times (a) $t = 1$ ps, (b) $t = 5$ ps, (c) $t = 10$ ps, (d) $t = 15$ ps, and (e) $t = 20$ ps. Fig. 10 shows normal stress

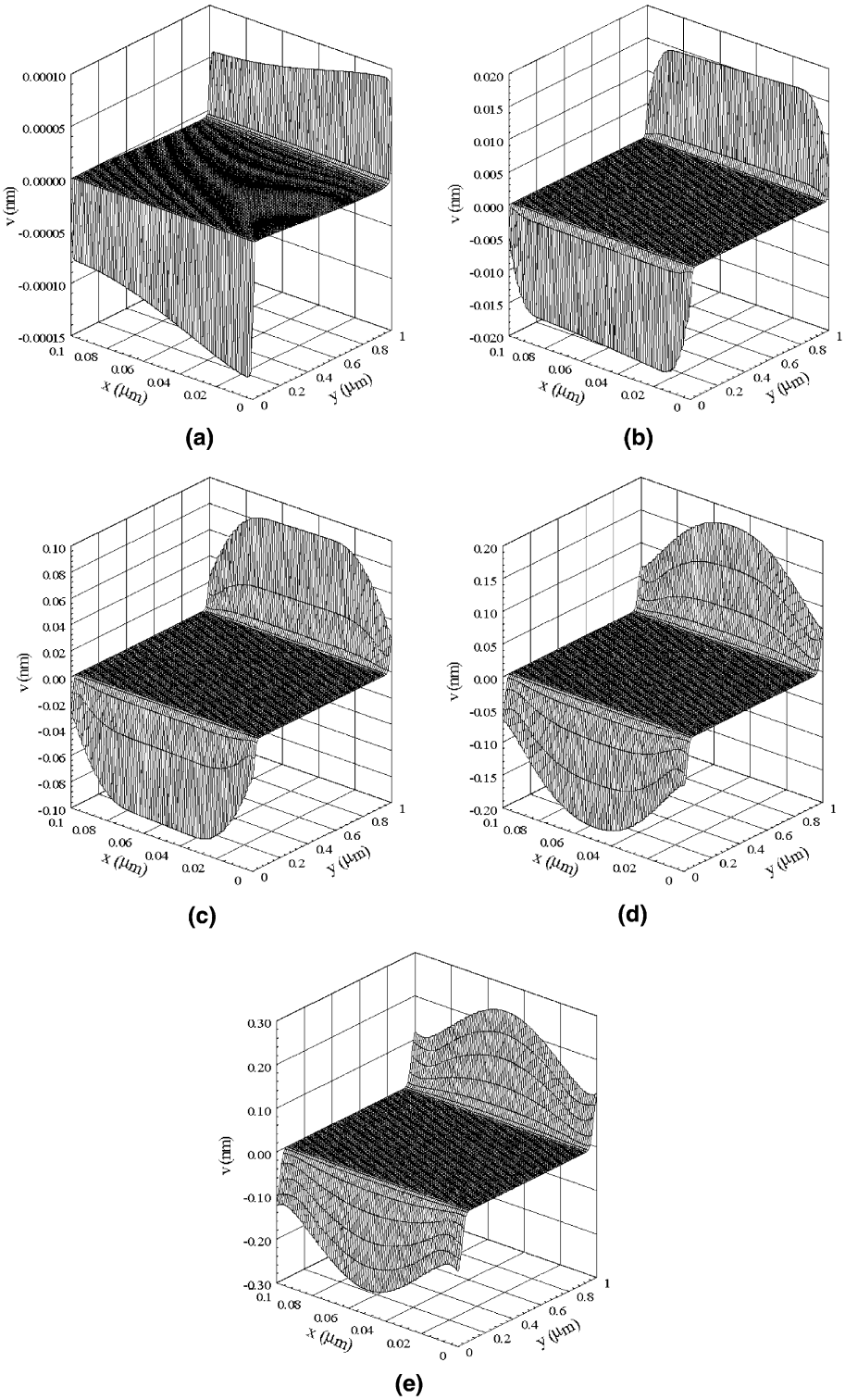

Fig. 9. Displacement (v) profiles at (a) $t = 1$ ps, (b) $t = 5$ ps, (c) $t = 10$ ps, (d) $t = 15$ ps, and (e) $t = 20$ ps.

σ_x (thickness direction) profiles at different times (a) $t = 1$ ps, (b) $t = 5$ ps, (c) $t = 10$ ps, (d) $t = 15$ ps, and (e) $t = 20$ ps. Fig. 11 shows normal stress σ_y (length direction) profiles at different times (a) $t = 1$ ps, (b) $t = 5$ ps, (c) $t = 10$ ps, (d) $t = 15$ ps, and (e) $t = 20$ ps. The analysis of displacement and stress waves reveals the significance of the hot-electron-blast effect on the ultrafast deformation mainly along the thickness direction. Furthermore, the proposed methodology allows us to obtain the solution free from non-physical oscillations.

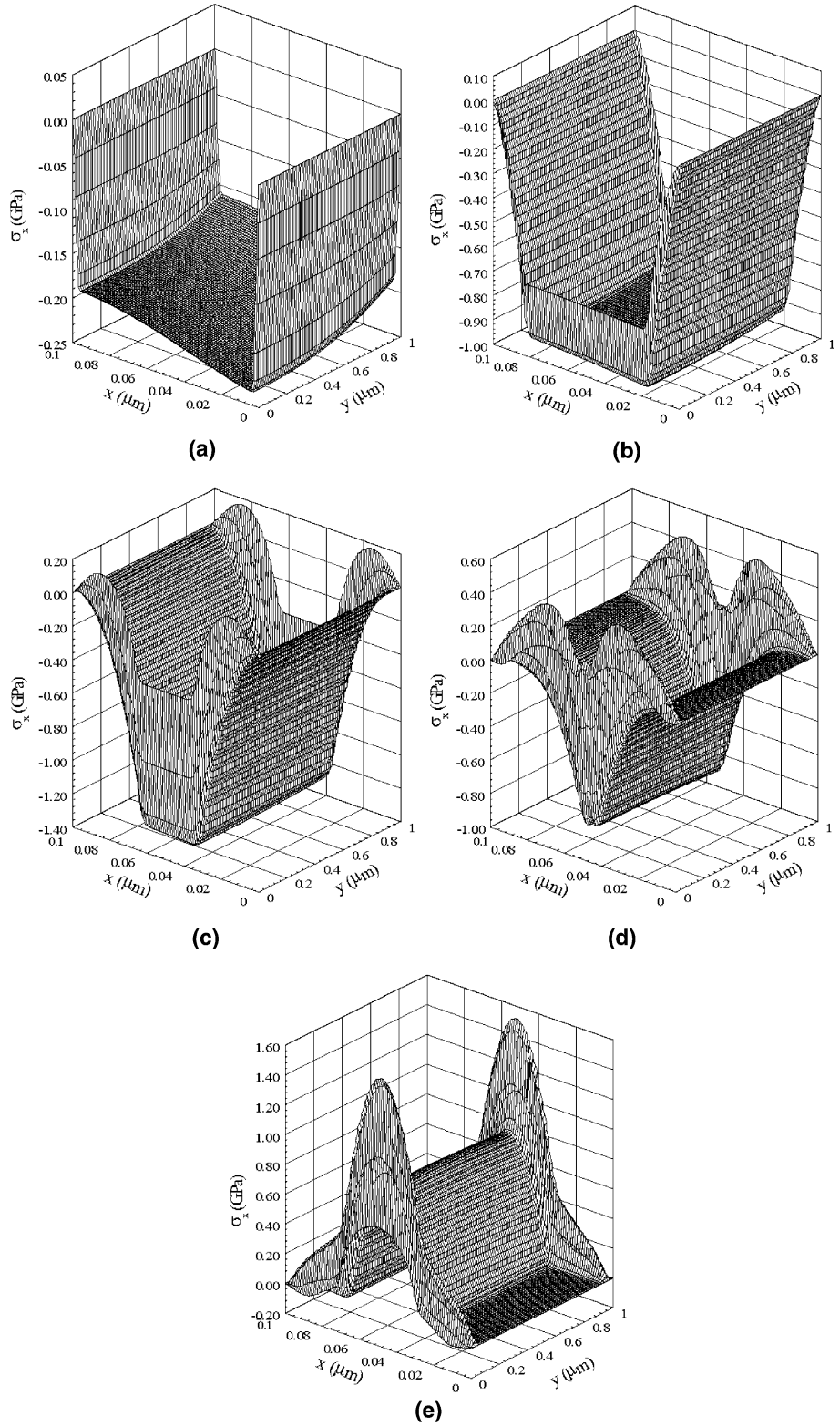

Fig. 10. Normal stress (σ_x) profiles at (a) $t = 1$ ps, (b) $t = 5$ ps, (c) $t = 10$ ps, (d) $t = 15$ ps, and (e) $t = 20$ ps.

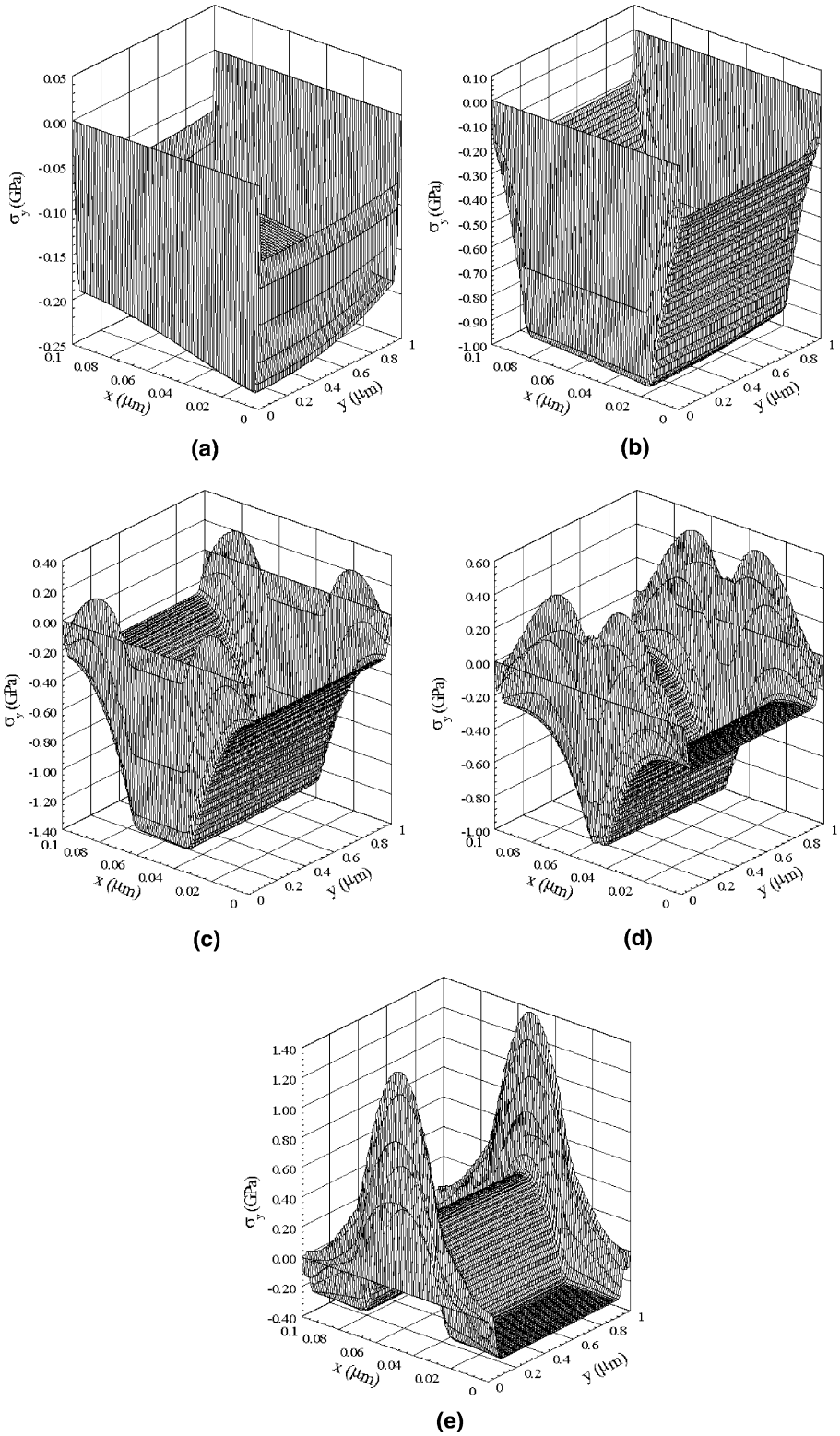

Fig. 11. Normal stress (σ_y) profiles at (a) $t = 1$ ps, (b) $t = 5$ ps, (c) $t = 10$ ps, (d) $t = 15$ ps, and (e) $t = 20$ ps.

5. Conclusion

We have developed a finite difference method for studying thermal deformation in a thin film exposed to ultrashort-pulsed lasers. The method, based on the parabolic two-step heat transport equations, accounts for the coupling effect between lattice temperature and strain rate, as well as for the hot-electron-blast effect in momentum transfer. By replacing the displacement components in the dynamic equations of motion using the velocity

components, and employing a staggered grid, we have developed a numerical method that allows us to avoid non-physical oscillations in the solution, as illustrated by a series of numerical experiments.

References

[1] D.Y. Tzou, J.K. Chen, J.E. Beraun, Hot-electron blast induced by ultrashort-pulsed lasers in layered media, Int. J. Heat Mass Transfer 45 (2002) 3369–3382.

[2] A. Mandelis, S.B. Peralta, Thermal wave based materials characterization and nondestructive evaluation of high-temperature superconductors: a critical review, in: R. Kossowsky (Ed.), Physics and Materials Science of High Temperature Superconductors II, Kluwer Academic publishers, Boston, MA, 1992, pp. 413–440.

[3] J. Opsal, The application of thermal wave technology to thickness and grain size of aluminum films, in: Metallization: Performance and Reliability Issues for VLSI and ULSI, SPIE 1596 (1991) 120–131.

[4] D.J. Elliot, B.P. Piwczyk, Single and multiple pulse ablation of polymeric and high density materials with excimer laser radiation at 193 nm and 248 nm, Mater. Res. Soc. Symp. Proc. 129 (1989) 627–636.

[5] C.P. Grigoropoulos, Heat transfer in laser processing of thin films, in: C.L. Tien (Ed.), Annual Review of Heat Transfer, vol. V, Hemisphere, New York, 1994, pp. 77–130.

[6] J. Narayan, V.P. Gosbole, G.W. White, Laser method for synthesis and processing of continuous diamond films on nondiamond substrates, Science 52 (1991) 416–418.

[7] J.M. Hopkins, J. Sibbett, Ultrashort-pulse lasers: big payoffs in a flash, Sci. AM 283 (2000) 72–79.

[8] J. Liu, Preliminary survey on the mechanisms of the wave-like behaviors of heat transfer in living tissues, Forschung im Ingenieurwesen 66 (2000) 1–10.

[9] C. Momma, S. Nolte, B.N. Chichkov, F.V. Alvensleben, A. Tunnermann, Precise laser ablation with ultrashort pulses, App. Surf. Sci. 109 (1997) 15–19.

[10] M.D. Shirk, P.A. Molian, A review of ultrashort pulsed laser ablation of materials, J. Laser Appl. 10 (1998) 18–28.

[11] A.N. Smith, J.L. Hostetler, P.M. Norris, Nonequilibrium heating in metal films: an analytical and numerical analysis, Numer. Heat Transfer, Part A 35 (1999) 859–873.

[12] K. Fushinobu, L.M. Phinney, Y. Kurosaki, C.L. Tien, Optimization of laser parameters for ultrashort-pulse laser recovery of stiction-failed microstructures, Numer. Heat Transfer, Part A 36 (1999) 345–357.

[13] J.K. Chen, J.E. Beraun, Numerical study of ultrashort laser pulse interactions with metal films, Numer. Heat Transfer, Part A 40 (2001) 1–20.

[14] E. Hoashi, T. Yokomine, A. Shimizu, Numerical analysis of ultrafast heat with phase change in a material irradiated by an ultrashort-pulsed laser, Numer. Heat Transfer, Part A 41 (2002) 783–801.

[15] S.H. Lee, J.S. Lee, S. Park, Y.K. Choi, Numerical analysis on heat transfer characteristics of a silicon film irradiated by pico-to femtosecond pulse lasers, Numer. Heat Transfer, Part A 44 (2003) 833–850.

[16] S.H. Lee, K.G. Kang, Numerical analysis of electronic transport characteristics in dielectrics irradiated by ultrashort-pulsed laser using the nonlocal Fokker–Planck equation, Numer. Heat Transfer, Part A 48 (2005) 59–76.

[17] J.K. Chen, W.P. Latham, J.E. Beraun, Axisymmetric modeling of femtosecond-pulse laser heating on metal films, Numer. Heat Transfer, Part B 42 (2002) 1–17.

[18] B. Xu, B.Q. Li, Finite element solution of non-Fourier thermal wave problems, Numer. Heat Transfer, Part B 44 (2003) 45–60.

[19] B.R. Barron, W. Dai, A hybrid FE-FD scheme for solving parabolic two-step micro heat transport equations in an irregularly shaped three-dimensional double-layered thin film, Numerical Heat Transfer, Part B, in press.

[20] I. Kaba, W. Dai, A stable three-level finite difference scheme for solving the parabolic two-step model in a 3 D micro-sphere heated by ultrashort-pulsed lasers, J. Comput. Appl. Math. 181 (2005) 125–147.

[21] W. Dai, G. Li, R. Nassar, L. Shen, An unconditionally stable three-level finite difference scheme for solving parabolic two-step micro heat transport equations in a three-dimensional double-layered thin film, Int. J. Numer. Meth. Eng. 59 (2004) 493–509.

[22] J.K. Chen, D.Y. Tzou, J.E. Beraun, Numerical investigation of ultrashort laser damage in semiconductors, Int. J. Heat Mass Transfer 48 (2005) 501–509.

[23] J.K. Chen, J.E. Beraun, C.L. Tham, Comparison of one-dimensional and two-dimensional axisymmetric approaches to the thermomechanical response caused by ultrashort laser heating, J. Opt. A: Pure Appl. Opt. 4 (2002) 650–661.

[24] J.K. Chen, J.E. Beraun, C.L. Tham, Investigation of thermal response caused by pulse laser heating, Numer. Heat Transfer, Part A 44 (2003) 705–722.

[25] J.K. Chen, J.E. Beraun, D.Y. Tzou, Thermomechanical response of metal films heated by ultrashort-pulsed lasers, J. Therm. Stresses 25 (2002) 539–558.

[26] S.D. Brorson, J.G. Fujimoto, E.P. Ippen, Femtosecond electron heat transfer dynamics in thin gold film, Phys. Rev. Lett. 59 (1987) 1962–1965.

[27] H. Reismann, P.S. Pawlik, Elasticity, Theory and Applications, Wiley, New York, 1980, p. 135.

[28] T.Q. Qiu, C.L. Tien, Short-pulse laser heating on metals, Int. J. Heat Mass Transfer 35 (1992) 719–726.

[29] S.V. Patanka, Numerical Heat Transfer and Fluid Flow, McGraw-Hill, New York, 1980 (Chapter 5).

[30] T.Q. Qiu, C.L. Tien, Short-femtosecond laser heating of multi-layer metals I. Analysis, Int. J. Heat Mass Transfer 37 (1994) 2789–2797.

[31] G.W.C. Kaye, Tables of Physical and Chemical Constants and Some Mathematical Functions, 14th ed., Longman, London, UK, 1973, p. 31.